Effect of powder metallurgy synthesis parameters for pure aluminium on resultant mechanical properties

Jinghang Liu[1,2] & Javier Silveira[1,2] & Robert Groarke[1,2] & Sohan Parab[1,2] & Harshaan Singh[1,2] & Eanna McCarthy[1,2] &
Shadi Karazi[1,2] & Andre Mussatto[2] & Jared Houghtaling[1,2] & Inam Ul Ahad[1,2] & Sumsun Naher [1,3] &
Dermot Brabazon[1,2]

Abstract

In this work, pure aluminium powders of different average particle size were compacted, sintered into discs and tested for mechanical strength at different strain rates. The effects of average particle size (15, 19, and 35 μm), sintering rate (5 and 20 °C/min) and sample indentation test speed (0.5, 0.7, and 1.0 mm/min) were examined. A compaction pressure of 332 MPa with a holding time of six minutes was used to produce the green compacted discs. The consolidated green specimens were sintered with a holding time of 4 h, a temperature of 600 °C in an argon atmosphere. The resulting sintered samples contained higher than 85% density. The mechanical properties and microstructure were characterized using indentation strength measurement tests and SEM analysis respectively. After sintering, the aluminium grain structure was observed to be of uniform size within the fractured samples. The indentation test measurements showed that for the same sintering rate, the 35 μm powder particle size provided the highest radial and tangential strength while the 15 μm powder provided the lowest strengths. Another important finding from this work was the increase in sintered sample strength which was achieved using the lower sinter heating rate, 5 °C/min. This resulted in a tangential stress value of 365 MPa which was significantly higher than achieved, 244 MPa, using the faster sintering heating rate, 20 °C/min.

Keywords Aluminium . Powder metallurgy (P/M) . Indentation . Sintering . Green compaction

Introduction

Pure aluminium has many important applications in consumer products, electrical and electronic engineering, and structural engineering [1–4]. In consumer products, aluminium is most noted in packaging applications. Due to its effect as an impermeable barrier and its non-toxicity, pure aluminium is widely used in packaging applications [5, 6]. Aluminium is one of the lightest engineering metals, having a strength to weight ratio superior to steel, however alloying with other elements is necessary to provide the higher strengths needed for structural applications. In this study, aluminium alloys with less than 1% alloying elements are considered as pure aluminium. Aluminium alloys based around pure aluminium predominantly, are used in automotive, aerospace, and shipbuilding industries [7–9] . Due to its unique visco-elastic mechanical response, nearly pure aluminium alloy EN-AW 1050A H24 has recently been proposed as structural shock load absorbing elements in building construction in areas of seismic activity [3]. The chemical composition of Al 1050A H24 has commercial denomination of Al 99.50% with alloying elements 0.07%Zn, 0.02%Ti, 0.02% others and has 0.02%Cu, 0.40%Fe, and 0.31%Si impurities [3].

In electrical engineering, pure aluminium is used instead of copper in power line applications due to it being more than three times less dense. While aluminium delivers 65% the conductivity of copper, it provides double the conductivity for the same weight of material. The strongly protective aluminium oxide layer also results in lower maintenance costs compared to other metallic alternatives. Due to its ductility, aluminium can be more easily drawn into long thin wires and

the high recyclable nature of aluminium also promotes it use in many applications [10–12]. Electrical components such as capacitors, rectifiers, as well as semiconductor compounds, e.g. AIIIBV, microprocessors, cryoelectronics, and satellite dishes are also produced with pure aluminium [12–14]. Other applications of pure aluminiuminclude mirror reflectors and as a structural material in nuclear reactors [15, 16]. Here in this contribution, we present a study on the mechanical strength of pure aluminium compacts produced using cold compaction followed by inert atmosphere furnace sintering. The powder metallurgy route of cold compaction followed by furnace sintering was recently used to provide densities of sintered specimens at 88% [17]. A number of

studies have been performed to reduce the high number of steps required by HIP, hot extrusion, vacuum hot pressing and hot-rolling [18–22], nevertheless the cold P/M route is preferential for providing pure and exact materials compositions, without the need for a high-cost facility. The P/M route can produce near net shape components with fine and uniform microstructure [23]. It can also provide better thermal stability as well as increased corrosion and tribological properties compared to alternative production techniques [24]. However, a number of complexities need to be overcome during the process of direct pure aluminium powder compaction and sintering. These complexities arise mainly because of the existence of a firm and intense oxide layer covering the powder particles. This oxide layer leads to a reduction in both compressibility, thermal conductivity and ultimately in the ability to sinter these powders [25].

For a specific P/M processing method, the strength of pure aluminium compacts must be established as a base point of comparison before final applications and including applications requiring reinforcement are examined. This would provide a better fundamental understanding of how these additions can contribute to the overall material properties and final applications of these P/M parts as light, corrosion resistant, or strong high temperature materials. As such the main objective of this study was to synthesis pure aluminium disk specimens with powder metallurgy and correlate the process parameters with the resulting mechanical properties.

Experimental procedure

Materials

Aluminium powders with an average particle size of 15 μm, 19 μm and 35 μm were purchased from commercial sources (Goodfellow Ltd. and East Coast Supplies Ltd.) as shown in Fig. 1 and detailed in Table 1. Confirmatory particle size measurements were performed using a Malvern Mastersizer S.

With the as-received pure powder, disk shaped specimens were made using cold compaction and consolidation sintering. D_{90} values for this powder were found to be <60 μm. All experimental measurements were recorded three times, $n = 3$. Average results values and 95% confidence intervals were calculated and presented.

Aluminium powder metallurgy

During placement of the powder into the die for cold compaction, the powder particles were gently vibrated to provide better packing and thereby decreased porosity. The pressure was gradually increased to the set level. During compaction the individual particles are deformed and cold welded which gives rise to the green compact strength [24]. The value of green density generally increases with increased compaction pressure and better packing. It has been reported previously that full density could be achieved with aluminium alloy powders at a sufficiently high compaction pressure [26]. Unalloyed atomised aluminium powders (< 20 μm) have also been reported to be consolidated to 100% density with a pressure of 1 GPa [23]. Higher green density after compaction enables the sintering process to proceed more efficiently. For the aluminium samples, a uniaxial hydraulic press (George E Moore and Son, Birmingham, UK) was used to produce the green compacts. The cylindrical die and resulting thin

cylindrical shapes were formed as shown in Fig. 2. For each compaction, 1.5 g of powder was compacted which resulted in a 1.5 mm thick samples with a diameter of 26 mm. All of the samples were produced at room temperatures between 18 and 25 °C. The compaction force applied for six minutes was 176 kN corresponding to a pressure of 332 MPa. This pressure limit was chosen in order to avoid damage to the die and sample during extraction. From a study of collaborating industry partner facilities, it was found that this pressure level would also be possible to implement within their facilities. Compaction and forming processes have been developed to deliver much higher pressures such as in the work of Wideroe et al. [22] and in the ECAP process [27], however most commercial and research forming machines work at much lower pressure levels [28]. Rhombic boron nitride powder as lubricant was physically dusted onto the mould wall to avoid the edge cracking of the green compacts during the demoulding process.

The theoretical solid density of pure aluminium is 2.7 g/cm3 while that of the loose powder used in this research is about 1.43 g/ml (approx. 70 ml for every 100 g of aluminium powder). The density of the green samples was measured by Archimedes method. For a higher applied pressure, a higher green density would be expected to result. For the pressures used in this study, the sintered densities obtained at the maximum pressure of 332 MPa were measured as 85.2%. Pure aluminium can be sintered in nitrogen, dissociated ammonia,
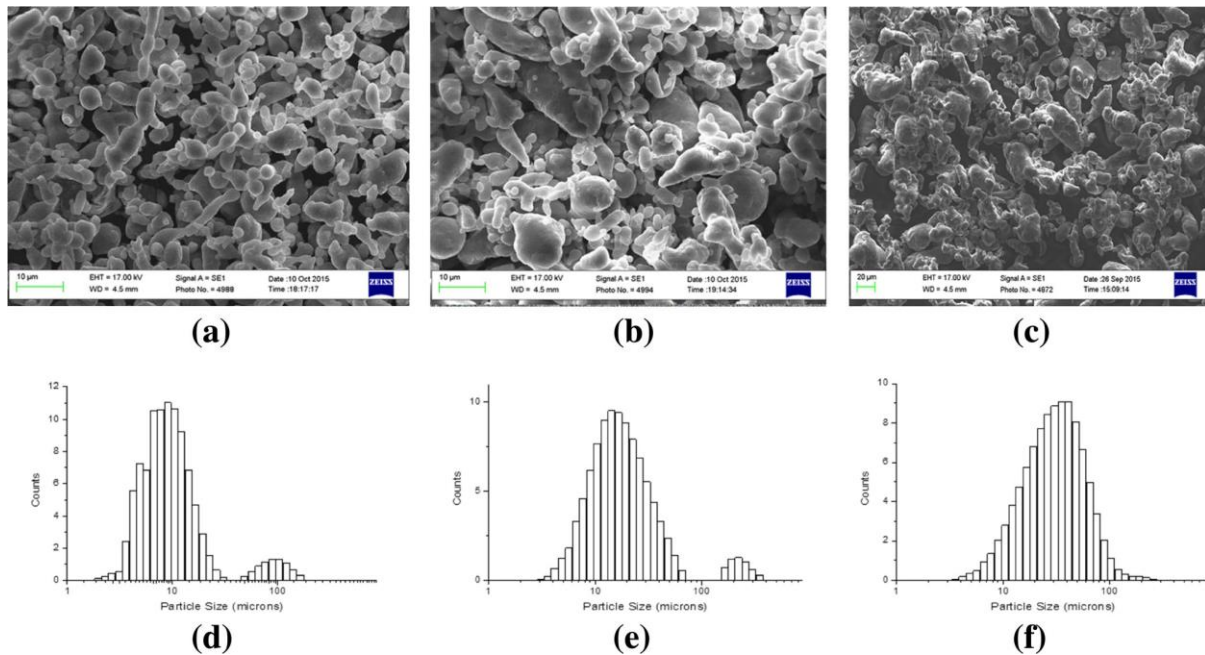

Fig. 1 Scanning electron micrographs of aluminium particles of a Goodfellow aluminium powder with mean particle size of 15 μm, b Goodfellow aluminium powder with mean particle size of 19 μm, c East Coast Fibreglass aluminium powder with mean particle size of 35 μm and with mixed morphology; size distributoins of d the 15 μm mean powder particle size, e the 19 μm mean powder particle size, and f the 35 μm mean powder particle size

argon, or vacuum [29]. For the DTA, a 20 °C/min ramp rate in argon atmosphere was applied to the maximumtemperature of 900 °C while the measurements were taken at one second intervals. The as-received aluminium powder of 15 μm, 19 μm and 35 μm particles sizes melted at temperature of 675 +/−4 °C. The oxidation and liquidus temperatures of the

powders used were firstly determined using differential thermal analysis (DTA), Stanton Redcroft DTA, as shown in Fig. 3.

The nominal melting point for pure aluminium is 660.3 °C but this value is influenced by many factors, including the oxide content, the particle size, and the purity of powder. Based on the DTA results, the selected sintering temperature was 600 °C (slightly less than 90% of the melting temperature), which meets the Brule of thumb^ that the sintering temperature is usually set between 70% and 90% of the melting point of the metal. It is well known that insufficient sintering time, overly fast heating rate or short sintering holding time can cause insufficient diffusion within the sintered aluminium specimens [25]. To accomplish sintering of the compacted samples presented in this work, a horizontal tube furnace, Carbolite model 3216 with Eurotherm temperature controller was used. Green samples were positioned in center of the furnace and the temperature of furnace was ramped up from room temperature at a rate of 20 °C/min (or 5 °C/min for comparison purpose) until the maximum temperature, 600 °C (88% of the melting temperature) was reached. The maximum temperature was held for 4 h, and the furnace was then naturally cooled to room temperature. In this study, an argon inert atmosphere was used during sintering which resulted in well-sintered samples. After sintering, disk samples as shown in Fig. 4 were produced.

Specimen characterization
### Indentation testing of disk samples
After the sintered disk samples of the different particle sizes were fabricated, they were indentation tested with a five

Table 1 Measured particle size and specifications of the aluminium powders investigated

Material	Source	Particle Size (μm)	Purity
Powder #1	Goodfellow Cambridge Ltd.	15 ± 3.3	99.00%
Powder #2		19 ± 5.9	
Powder #3	East Coast Supplies Ltd. (250mesh)	35 ± 1	99.50%
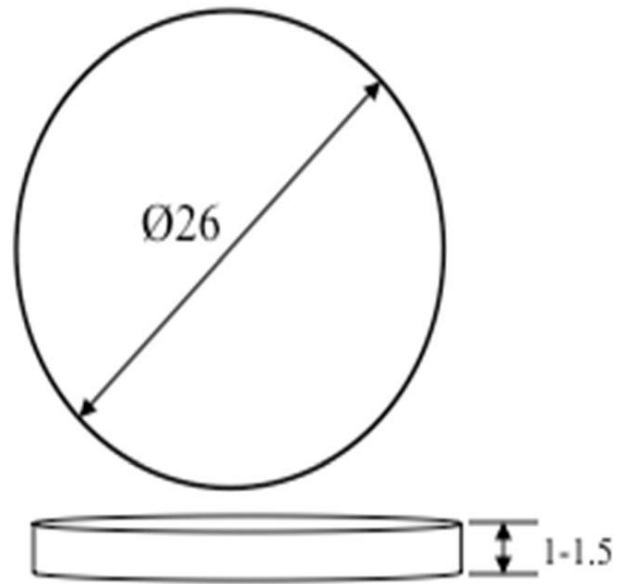
Fig. 2 a Picture of compaction mould and b schematic of produced specimen dimensions (mm)

millimeter protrusion indenter on a Zwick Roell, UK, universal testing machine (Z005, T1-FR005TN.A50), as shown in Fig. 5a. Figure 5b shows some of the samples post testing. Three loading velocities were examined during these tests, 0.5, 0.7 and 1 mm/min.

Based on the force recorded by the load cell, the sample deflection of the disk can be calculated from the process parameters using Eq. 1 [30],

$$y = \frac{3PR^2}{4\pi E t^3} (3 + v)(1-v) \quad (1)$$

where y is the deflection in the sample centre, P is the vertical load in central point, R is the radius of the circular solid disk, t represents the thickness of disk, E is Young's modulus of the aluminium (70 GPa), and v equals to the Poisson's ratio of aluminium (0.35). The radial stress σ_r and tangential stress σ_t can be calculated via Eqs. 2 and 3 as follows,

$$\sigma_r = \frac{3P}{2\pi t^2}(1+v)\log\frac{R}{x} = 0.31P \quad (2)$$

$$\sigma_t = \frac{3P}{2\pi t^2}\left[(1+v)\log\frac{R}{x} + (1-v)\right]$$

¼ 0:51P ð3Þ

where x represents the diameter of the indenter. The axial
stress σ_a was neglected in comparison to the radial and tangential
stress [30, 31]. Based on these equations stress values
were calculated and plotted against displacement, see Fig. 6.
Recorded fracture displacements and corresponding radial
and tangential stress values are listed in Table 2. Aluminium
particle size and sintering rate both had influence on the displacement
at which fracture occurred as well as on the corresponding
radial and tangential stress. For example, with
0.5 mm/min testing speed, the 35 μm powder particle size
provided the largest displacement before failure while the
15 μm average particle samples gave the smallest displacement.
It was also observed that a significantly higher radial
and tangential stress were achieved (221 MPa and 365 MPa
respectively) for the samples with 35 μm mean particle size
which were prepared with a sintering rate of 5 °C/min and
tested with an indentation rate of 0.5 mm/min, in comparison
to the smaller staring particle sizes. The fracture displacements
of the samples are shown in Fig. 7 and the radial and tangential
stresses are shown in Fig. 8. The 35 μm mean particle size
produced samples with sintering rate of 5 °C/min provided the
highest strength samples under all testing velocities. The
35 μm powder which contained a mixed morphology and
wider size distribution, had significantly improved ductility
due to reduced porosity, as observed from SEM images, in
the compacted and sintered sample structure. The lower
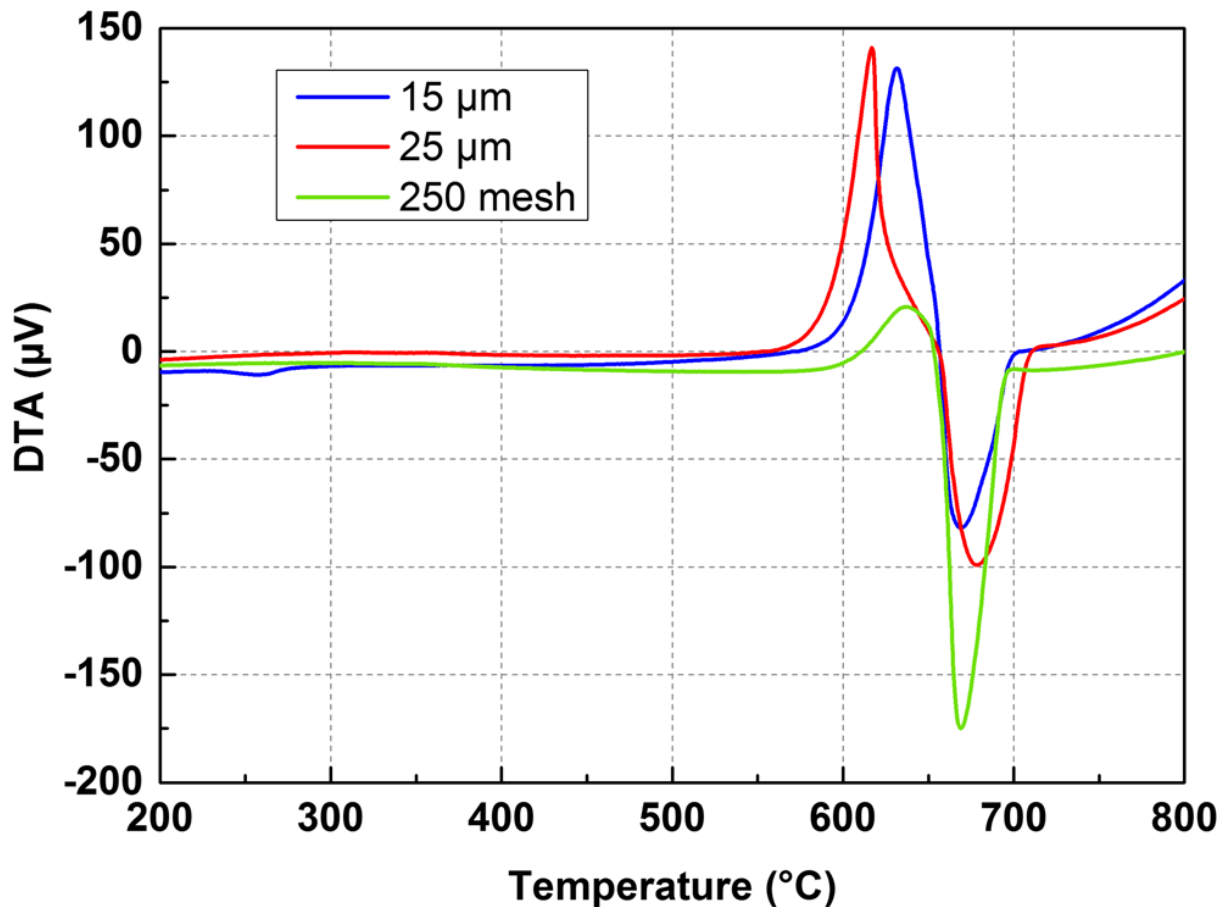sintering rate repeatedly resulted in increased sample strength

Fig. 3 Differential readings against the temperature of the aluminium powders

(a)   (b)

Fig. 4 a Picture of ceramic tundish with pure aluminium disk samples after compaction and sintering: 1.5 g aluminium powder with argon at a flow rate 1.5 mL/min, temperature of 600 °C, and a holding time 4 h; and b enlarged picture of disk samples in (a)

relative to the higher sintering rate of 20 °C/min.

Fracture structure characterisation

The dimpled fracture surfaces of the disk samples, indicating good sample sintering and ductility, are shown in Fig. 9.

Results and discussion

In this work, the P/M route was used to produce pure aluminium disk samples from powders of mean particle size 15 μm, 19 μm and 35 μm. For green samples made from these powders, the compaction quality was influenced by compaction pressure, holding time, lubrication method, and powder quantity. The green sample quality, as measured by porosity, starts to deteriorate under insufficient pressure or by compaction with an uneven powder surface. These conditions result in final samples which are relatively fragile and brittle. The cold compaction and sintering process developed in this work produced relatively defect free disks by using a high compaction pressure (332 MPa) and a holding time of six minutes. The density obtained for the 35 μm powder at the pressure of 332 MPa was measured as 85.2%. Stress values were very reproducible up to the cracking point, giving a strong baseline for comparison within this and future work, both for

unmodified aluminium and aluminium composite systems [32–34]. The peak tangential stress values observed ranged from 137 MPa to 365 MPa. It was observed that the significant higher radial and tangential stress were achieved for the 35 μm mean powder particle size samples produced with the lower heating rate of 5 °C/min.

Robust sintering was achieved from the three aluminium particle sizes, as was observed from the analysis of the SEM images obtained for each surface. The SEM images of the lower particle size fracture sample surfaces, Fig. 9a, b showed more porous surfaces than was observed from the samples produced from the larger particle size, see Fig. 9c. The indentation load which lead to these fracture surfaces was applied centrally in the disk test specimens. There is a clear dimpled structure in the fractographs shown in Fig. 9a, b. These fracture structures are typical of those seem in the literature [35] and represent ductile material fracture where the pores are nucleated from dislocation build up at grain boundaries, followed by pore joining, and eventually to the point where the stress level is sufficient to break the remaining connected material. The samples produced with the larger 35 μm average size particle showed higher levels of ductility and load bearing capability. The associated greater extent of fracture surface shearing and lower amount of dimpling is evident in this fracture surfaces, see Fig. 9c.

Fig. 5 a Picture of indentation test configuration, and b disk samples after indentation testing; from top to bottom row, specimens are of 15 μm, 19 μm, and 35 μm powder, while from left to right column, test speeds represented are 0.5, 0.7 and 1 mm/min
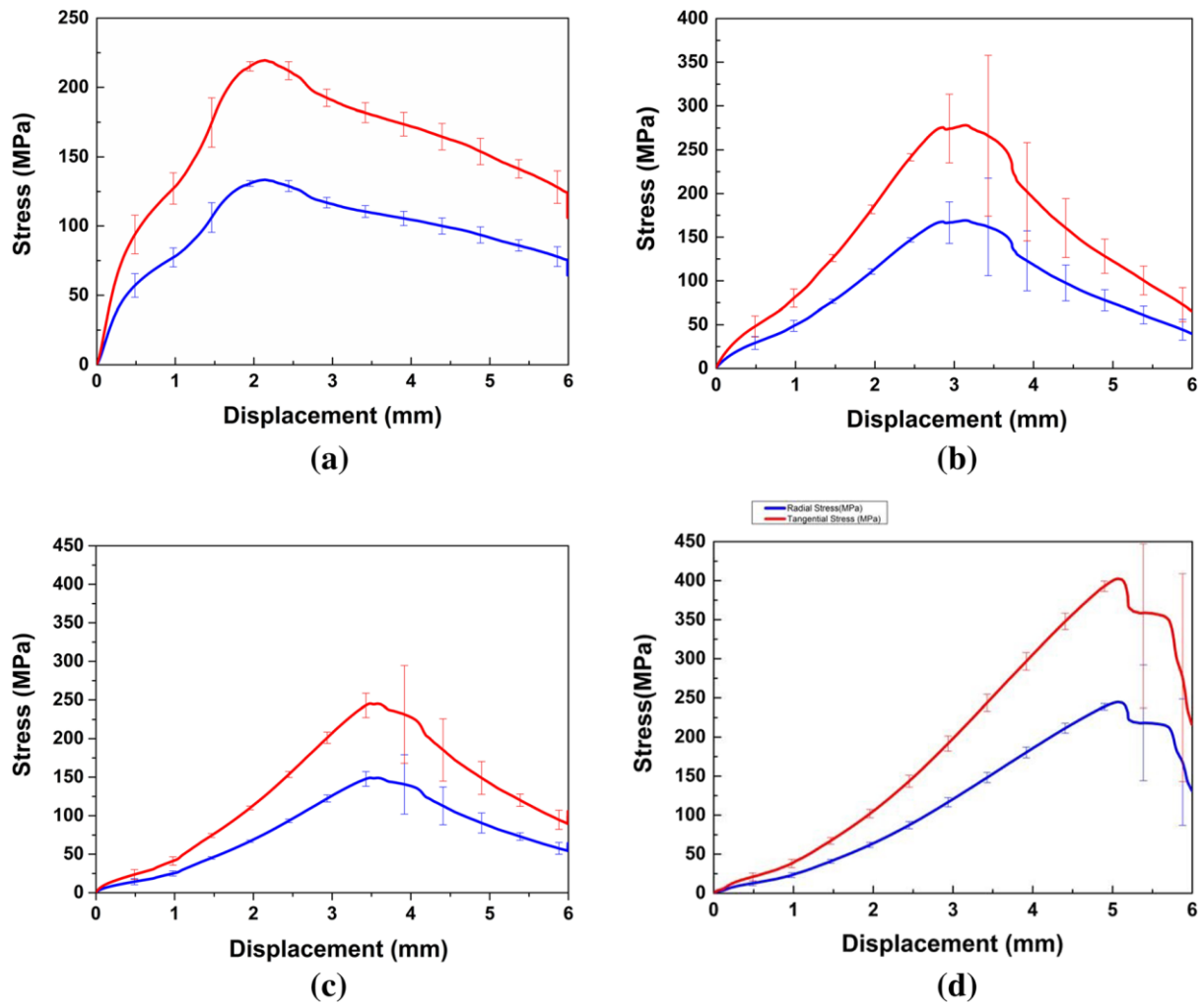

(a)   (b)
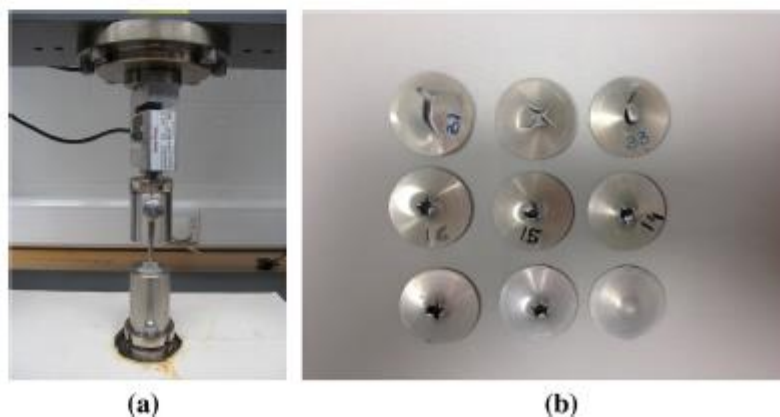
Fig. 6 Stress versus displacement of pure aluminium samples of particle size a 15 μm, b 19 μm, c 35 μm sintered at 20 °C/min, and d 35 μm sintered at 5 °C/min. Radial stress and tangential stress are represented by blue and red lines respectively, n = 3

The mechanical strength of the samples was found to be dependent on the sintering heating rate. The highest radial and tangential strengths were found for the largest particle size and the lower heating rate of 5 °C/min. It is conjectured that the lower heating rate allowed time for atomic diffusion. Indentation testing results from the samples with the 35 μm particles sintered using a heating rate of 5 °C/min exhibited the highest ductility and load bearing capability (400 MPa at 5 mm) across the three loading rates tested. The error bars are however higher for the 35 μm particle samples produced with a sintering rate of 5 °C/min. The increased error bars for the slow heating rate are presumed to be due to the enhanced period for gas adsorption and entrainment within the aluminium. Even small concentrations of gases such as oxygen adsorption could lead to significant increase in sample porosity and hence reduction in sample mechanical properties. The DTA results highlighted some variations in the melting temperature of the powders which may be associated to varying levels of sample purity and oxidation on the particles due to their varying surface area to volume ratios and the variance in the heat transfer through the crystal lattices of the samples by virtue of their differing particle sizes, melt pool uniformity

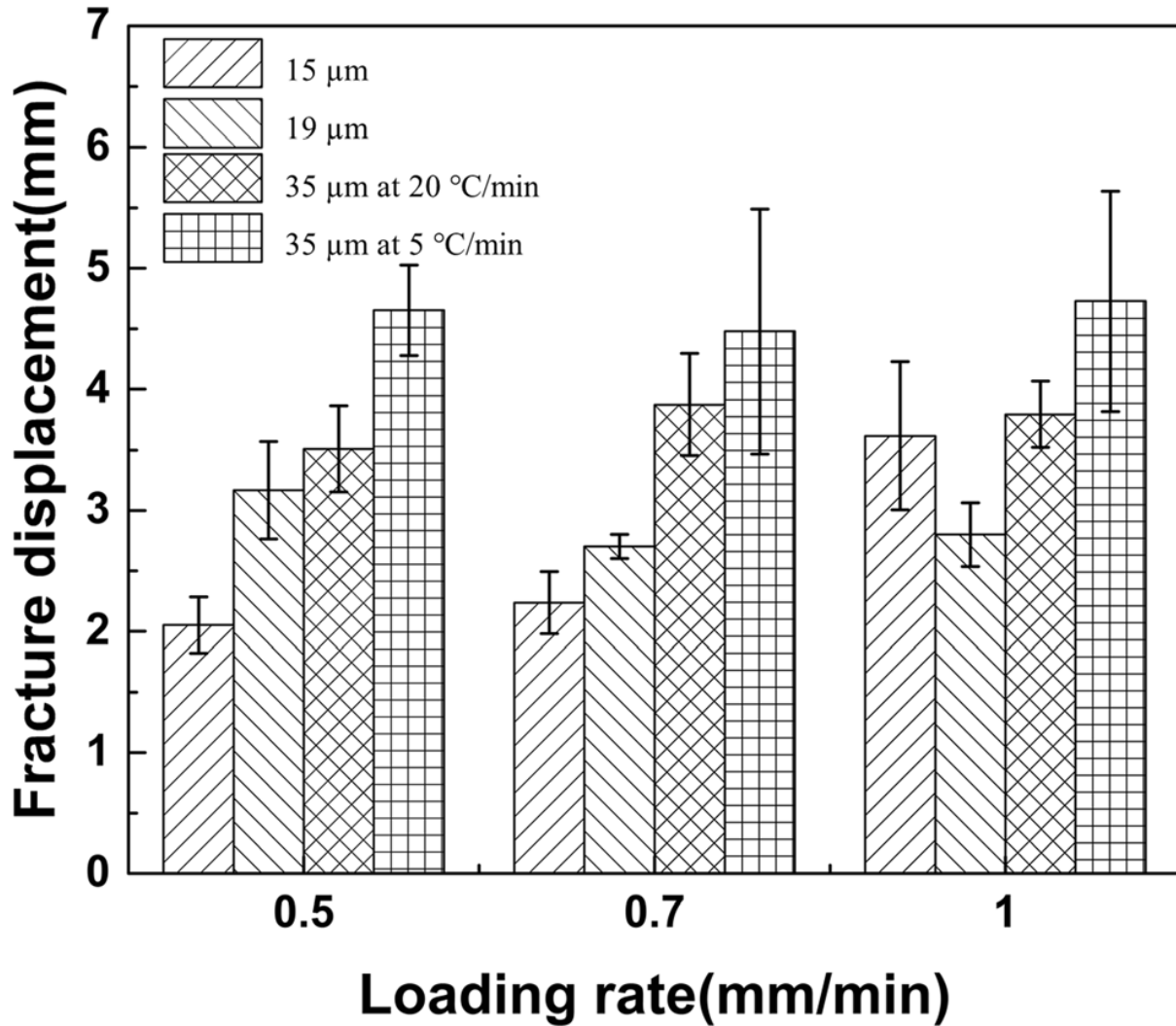| Testing speed of		0.5 mm/min	0.7 mm/min	1 mm/min
Particle size (μm)	Sintering rate (°C/min)	$[y, \sigma_r, \sigma_t]$ (mm, MPa, MPa)		
15	20	2.1, 135, 222	2.2, 138, 227	3.6, 84, 138
19	20	3.1, 186, 306	2.7, 149, 245	2.8, 177, 292
35	20	3.5, 148, 244	3.8, 171, 282	3.7, 157, 258
35	5	**4.6, 222, 365**	4.4, 199, 328	4.7, 219, 360

Fig. 7 Fracture displacement under the testing speed of 0.5, 0.7, and 1 mm/min. Default sintering rate for 15 μm, 19 μm and 35 μm powder was 20 °C/min; n = 3; 95% confidence intervals shown

and oxidation levels. The presence of oxygen and/or nitrogen in the environment during DTA analysis as well as the smaller grain sizes of the powders could also influence the melting temperature. Further work on detailed TGA and XPS analysis of these particle phase changes and their surfaces chemistries respectively would allow for a more fundamental understanding and confirmation of the underlying causes of these results.

Conclusion

In this work, pure aluminium compacts have been produced with a number of particle sizes and tested at a number of indentation speeds to establish their physical mechanical behaviour. To achieve stable green and sintered disk samples, the P/M technique of green compaction and sintering was optimized. Well-formed green samples and sintered specimen of

variable particle sizes were then obtained. The indentation results indicate that under the identical testing speed, that the 35 µmpowder at 5 °C / min sintering rate provided the highest radial and tangential strength, closely followed by the 35 µm powder at 20 °C /min sintering rate. This is considered to be due to the make-up of the 35 µm powder which had a mixed morphology and a wide particle size range. This significantly improved the material strength by reducing porosity in the consolidated and sintered structures. The lower surface area to volume ratio of the larger particles provides relatively more aluminium volume and a lower barrier to inter-particle atom diffusion and binding. Another important finding from this work is the increase in sintered compact strength which was achieved by using a lower heating rate. In this work, this resulted in a tangential stress value of 365 MPa which was significantly higher than for the faster sintering heating rate, 244 MPa. The reason for this is believed to be that the lower heating rate allowed increased time and hence extent of atomic diffusion between particles. The 15 µm powder sample provided the lowest strengths among all samples. This is likely due to the increased alumina to aluminium volume of the smaller particles making it more difficult for aluminium atomic diffusion between particles. The P/Mprocess on high purity aluminium powders examined in this paper presents processing conditions for obtaining pure aluminium samples of definable strength. The presence of a stable oxide layer is a major restriction in the exploitation of the conventional sintering process for smaller aluminium powder particles. However, methods of overcoming these problems can be implemented such as modification of surface oxide distribution,
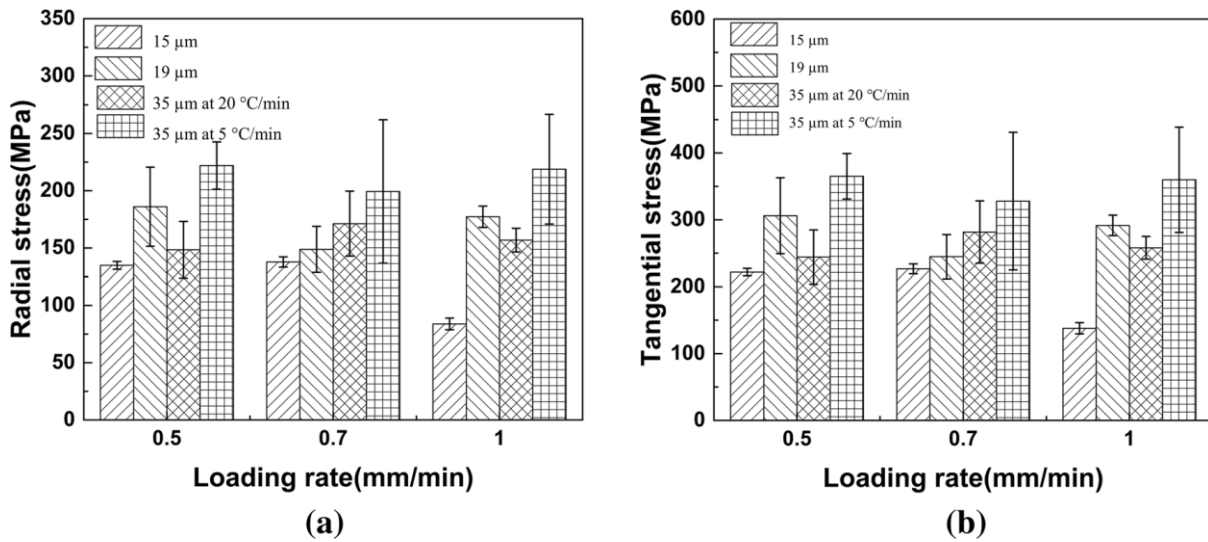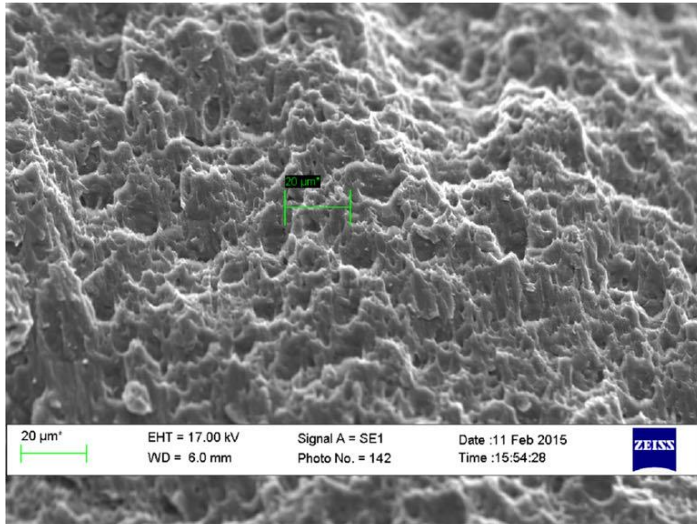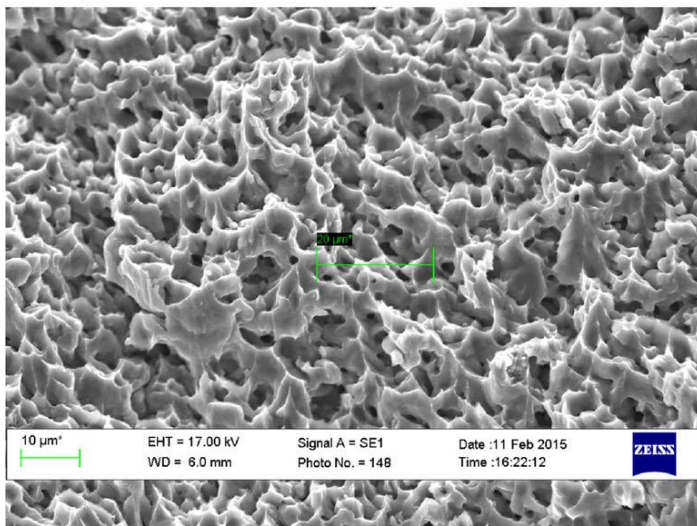

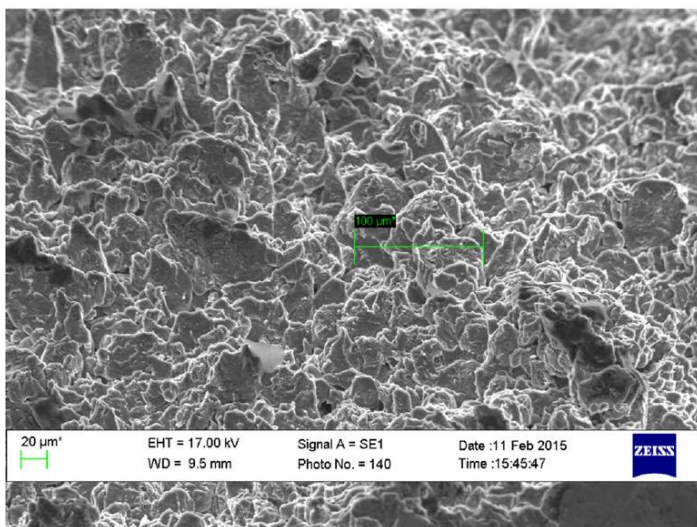Fig. 8 a Radial and b tangential stress under the testing speed of 0.5, 0.7, and 1mm/min. Default sintering rate for 15 µm, 19 µmand 35 µmpowder was 20 °C/min; n = 3; 95% confidence intervals shown

(a)

(b)

(c)

Fig. 9 SEM photos of fracture morphology on cross sections of disk samples prepared with a 15 μm, b 19 μm, and c 35 μm powder, indicating the disk samples were uniformly sintered

removal of stable surface oxides, and exploitation of the surface oxide chemistry. In future work, the combination of the controlled process as proposed in this paper with oxide reduction methods will be examined. For example, oxide concentration may be reduced using a fluxing agent such as acetamide, zinc chloride, or sodium fluoride [36]. The addition of magnesium is also known to disrupt the passivating oxide layer via the formation of a spinel phase [37]. These will be examined for the niche electrical and electronic applications of relatively pure metallic composites.

Compliance with ethical standards

Conflict of interest None.

References

1. Dursun T, Soutis C (2014) Recent developments in advanced aircraft aluminium alloys. Mater Des 56:862–871
2. Brandt R, Neuer G (2007) Electrical resistivity and thermal conductivity of pure aluminum and aluminum alloys up to and above the melting temperature. Int J Thermophys 28(5):1429–1446
3. De Matteis G, Brando G, Mazzolani FM (2012) Pure aluminium: an innovative material for structural applications in seismic engineering. Constr Build Mater 26(1):677–686
4. Hirsch J (2004) Automotive trends in Aluminium-the European perspective. Mater Forum 28:15–23
5. Soares B, Dantas S (2017) Corrosion of aluminum for beverage packaging in acidic media containing chlorides and copper ions. J Food Process Eng 40(6). https://doi.org/10.1111/jfpe.12571
6. Fasoyiro S, Gourama H, Cutter C (2017) Stability and safety of maize–legume-fortified flours stored in various packaging materials. Eur Food Res Technol 243:1861–1868
7. Zulkifli F, Ali N, Yusof MSM, KhairulWM, Rahamathullah R, Isa MIN,Wan NikWB (2017) The effect of concentration of Lawsonia Inermis as a corrosion inhibitor for aluminum alloy in seawater. Adv Phys Chem 2017. https://doi.org/10.1155/2017/8521623
8. Dudin M, Voykova N, Frolova E, Artemieva J (2017) Modern trends and challenges of development of global aluminum industry. Metalurgija 56(1–2):255–258
9. Mandal N (2017) Ship construction and welding. https://doi.org/10.1007/978-981-10-2955-4
10. Yu H, Li R, Qian M, Ma H, Hou J, Wang Q (2017) The development of high strength-high conductive aluminum conductors. Electrical Engineering and Automation 307–318. https://doi.org/10.1142/9789813220362_0039
11. Taguchi K, Akasofu Y, Yoshimoto J (2017) Development of high strength aluminum wires for low-voltage automotive wiring harnesses. SAE Int J Engines 10(4). https://doi.org/10.4271/2017-01-1644
12. Cui X, Wu Y, Zhang G, Liu Y, Liu X (2017) Study on the improvement of electrical conductivity and mechanical properties of low alloying electrical aluminum alloys. Compos Part B Eng 110:381–387
13. Cousseau R, Patin N, Forgez C,Monmasson E, Idkhajine L (2017) Improved electrical model of aluminum electrolytic capacitor with anomalous diffusion for health monitoring. Math Comput Simul 131:268–282
14. Du X, Lin B, Li B, Feng T, Mao S, Xu Y (2017) Surface modification of al foils for aluminum electrolytic capacitor. Adv Funct Mater 27(11):1606042
15. Wette J, Sutter F, Fernández-García A, Ziegler S, Dasbach R (2016) Comparison of degradation on aluminum reflectors for solar collectors due to outdoor exposure and accelerated aging. Energies 9(11):916
16. Mishra SK, Kumar V, Tiwari SK, Mishra T, Angula G, Adhikari S (2016) Development and degradation behavior of protective multilayer coatings for aluminum reflectors for solar thermal applications. Thin Solid Films 619:202–207
17. Liu J, O'Connor WJ , Ahearne E, Byrne G (2013) Electromechanical modelling for piezoelectric flextensional actuators.

Smart Mater Struct 23(2):1−13

18. Hsiang SH, Lin YW, Lai JW (2012) Optimization of hot extrusion process for AZ61 magnesium alloy carriers. Int J Mater Form 5(3): 259−268

19. Sornin D, Karch A, Nunes D (2015) Finite element method simulation of the hot extrusion of a powder metallurgy stainless steel grade. Int J Mater Form 8(1):145−155

20. Güley V, Ben Khalifa N, Tekkaya AE (2010) Direct recycling of 1050 aluminum alloy scrap material mixed with 6060 aluminum alloy chips by hot extrusion. Int J Mater Form 3(SUPPL. 1):853−856

21. Widerøe F, Welo T, Vestøl H (2010) A new testing machine to determine the behaviour of aluminium granulate under combined pressure and shear. Int J Mater Form 3(S1):861−864

22. Brosius A, Hermes M, Ben Khalifa N, Trompeter M, Tekkaya AE (2009) Innovation by forming technology: motivation for research. Int J Mater Form 2(S1):29−38

23. Totten GE, MacKenzie DS (2003) Handbook of aluminum: Vol. 1: Physical metallurgy and processes. Taylor & Francis, New York

24. Verlinden B, Froyen L (1994) Aluminium Powder Metallurgy. European Aluminium Association

25. Gökçe A, Fındık F (2008) Mechanical and physical properties of sintered aluminum powders. J Achiev Mater Manuf Eng 30(2): 157−164

26. Djuricic M, Dragojlovic M, Novakovic R (1986) Cold sintering of aluminum and its alloys. Sci Sinter 18:87−89

27. Sabirov I, Perez-Prado MT, Murashkin M, Molina-Aldareguia JM, Bobruk EV, Yunusova NF, Valiev RZ (2010) Application of equal channel angular pressing with parallel channels for grain refinement in Aluminium alloys and its effect on deformation behaviour. Int J Mater Form vol. 3, Suppl 1, pp 411−414

28. ElRakayby H, Kim K (2017) Effect of glass container encapsulation on deformation and densification behavior of metal powders during hot isostatic pressing. Int J Mater Form. https://doi.org/10.1007/s12289-017-1361-8

29. Okuma S (1979) The sintering mechanism of Aluminium and the anodization of Aluminium sintered bodies. Act Passive Electron Compon 6(1):23−29

30. Hearn EJ (1997) Mechanics of materials, volume 2-an introduction to the mechanics of elastic and plastic deformation of solids and structural materials, vol 2, 3rd edn. Elsevier, Amsterdam

31. Timoshenko S, Woinowsky-Krieger S (1959) Theory of plates and shells, engineering societies monographs.McGraw-Hill, New York

32. Liu J, Fernandez B, Rodriguez P, Naher S, Brabazon D (2016) Powder processing methodology for production of graphene oxide reinforced aluminium matrix composites. Advances in Materials and Processing Technologies 2(4):437−450. https://doi.org/10.1080/2374068X.2016.1244389

33. Liu J, Khan U, Coleman J, Fernandez B, Rodriguez P, Naher P, Brabazon D (2016) Graphene oxide and graphene nanosheet reinforced aluminium matrix composites: powder synthesis and prepared composite characteristics. Mater Des 94:87−94

34. Dasari B, Nouri JM, Brabazon D, Naher S (2017) Graphene and derivatives - synthesis techniques, properties and their energy applications. Energy 140:766−778

35. ASM Handbook (1987) Volume 12: Fractography. ISBN: 978−0−87170-018-6

36. Kowalski L, Korevaar BM, Duszczyk J (1992) Some new aspects of the theory of oxidation and degassing of aluminium-based alloy powders. J Mater Sci 27(10):2770−2780. https://doi.org/10.1007/BF00540704

37. Lumley RN, Sercombe TB, Schaffer GM (1999) Surface oxide and the role of magnesium during the sintering of aluminum. Metall Mater Trans A 30(2):457−463. https://doi.org/10.1007/s11661-999-0335-y